Journal of Catalysis 382 (2020) 385–394

Contents lists available at ScienceDirect

Journal of Catalysis

journal homepage: www.elsevier.com/locate/jcat

Solid solutions in reductive environment – A case study on improved CO_2 hydrogenation to methane on cobalt based catalysts derived from ternary mixed metal oxides by modified reducibility

Tanja Franken [a,1,*], Jasmin Terreni [b], Andreas Borgschulte [b], Andre Heel [a,2]

[a] Institute of Materials and Process Engineering (IMPE), Zurich University of Applied Sciences (ZHAW), Technikumstrasse 9, CH-8401 Winterthur, Switzerland
[b] Laboratory Advanced Analytical Technologies, EMPA- Swiss Federal Laboratories for Materials Science & Technology, Überlandstrasse 129, CH-8600 Dübendorf, Switzerland

ARTICLE INFO

Article history:
Received 23 September 2019
Revised 21 December 2019
Accepted 26 December 2019

Keywords:
CO_2 methanation
Spinel catalysts
Reducibility
Formate mechanism
Hydrogen spillover

ABSTRACT

Mixed metal oxides as solid solutions are promising catalyst precursor species, due to their atomic dispersion of metals within an oxide matrix. Upon activation by pre-reduction highly dispersed metal nanoparticles grow on the surface of a functional mixed metal support. Herein, the impact of different amounts of structure distorting manganese that is integrated in $CoMn_xAl_{2-x}O_4$ spinel phase on the reducibility as a measure for the ability for pre-activation was investigated. The reducibility of the spinel increases with increasing Mn content. By using the Sabatier reaction (CO_2 methanation) as model reaction it was shown that the activity depends on the low temperature reducibility of the spinel. The highest catalytic productivity of 0.65 mol/(mol·min) at 400 °C was obtained with $CoMn_{0.5}Al_{1.5}O_4$ as a precursor in line with a highly improved selectivity ($S(CH_4)$ = 97%) towards methane as compared to manganese free $CoAl_2O_4$. In addition, the activation energy drops from 107 kJ/mol to 69 kJ/mol upon Mn incorporation. Intense surface analysis via CO & H_2 pulsed titration, BET, CO_2-TPD, CO_2 DRIFTS, as well as *operando* DRIFTS analysis revealed, that the integration of Mn into the spinel support decreases the overall surface basicity and enables, potentially due to its Mn^{3+}/Mn^{2+} redox pairs, spillover of hydrogen from the metallic sites towards the surface of the support. This leads to an altered reaction mechanism via formate species without production of CO as reaction intermediates. This in combination with the ability to transfer the CO_2 conversion from the metal sites only towards the surface of the support due to hydrogen spillover leads to the observed increase in catalytic performance. This work demonstrates the high potential of specific modification of typically highly stable mixed metal oxides as valuable catalyst precursor species.

1. Introduction

One of the central issues of current society is the transition from a "throw-away-society" into a recycling economy in order to overcome the measurable impacts of climate changes and depleting resources. Atmospheric CO_2 concentration has risen from preindustrial level of 250 ppm to 400 ppm until today. This is due to continuous anthropogenic emission from fossil fuel combustion into the environment [1]. Reuse of CO_2 with renewable H_2 as a chemical feedstock for fuels would be a solution to transfer into a circular economy without changing all end consumers and energy transport facilities. So far, its economic reasonable recycling is limited to a few large and centralised sources, such as cement production or incinerator plants [2]. In the future separation from air becomes considerable [3–5]. Nevertheless, the production chain of renewable CO_2 based hydrocarbons (e.g. CH_4) relies on a hydrogenation process with high efficiency that enables CO_2 activation and transformation into valuable added energy carrier on efficient catalysts.

Even though Ni is the preferred choice of methanation catalyst, Co/Al_2O_3 catalysts are active in CO_2 reduction to CO, CH_4 and have the potential to produce longer chain carbohydrates via Fischer-Tropsch-reactions [6,7]. One of the main challenges of Co/Al_2O_3 catalysts is the proper interaction between the support and the Co species. On the one hand, interactions should be strong enough to stabilize Co particles. On the other hand, too strong metal support interactions limit the reduction to the active metallic Co

* Corresponding author.
E-mail address: tanja.franken@psi.ch (T. Franken).
[1] Present address: Paul Scherrer Institute PSI, Forschungsstrasse 111, CH-5232 Villigen PSI, Switzerland.
[2] Present address: Institute of Environmental and Process Engineering (UMTECH), University of Applied Sciences Rapperswil (HSR), Oberseestr. 10, CH-8640 Rapperswil, Switzerland

https://doi.org/10.1016/j.jcat.2019.12.045
0021-9517/

specie [8–10]. As a result oxidation of Co takes place on Co/Al_2O_3 catalysts and inactive spinel-type $CoAl_2O_4$ is formed that leads to limited catalytic performance [11–13]. On the other hand, looking at the spinel phase from another point of view, it can be considered as a well distributed solid solution, which in general have been reported as suitable catalyst precursor in order to generate highly active and finely dispersed metal nanoparticles [14]. But the reducibility of such Co-aluminate spinel needs to be improved in order to enable reactivation by growth of Co nanoparticles on the surface. Growth of metal nanoparticles on oxide surfaces in general was even proven to be reversible and repeatable on perovskites, if the crystalline structure stays intact upon reduction [15,16]. Spinels are versatile mixed metal oxides whose reducibility can be tailored by compositional modifications [17,18]. Thus, even though spinels are regarded as detrimental for the methanation reaction, highly active Co species could be created on the surface upon reduction, serving as active sites. Thus, a proper spinel modification might enable continuous reduction of the structure and reformation of active sites under CO_2 hydrogenation conditions. Mn is known to distort the structure of such spinels [19,20]. Hence, it should be capable to increase the reducibility of the Co-aluminate in order to use the spinel as a solid solution precursor. Concepts in literature to overcome deactivation so far rely on doping with relatively expensive noble metals such as Ru, Re and Pt [21–23].

Due to its simplicity, the Sabatier reaction (1) is used as model reaction at ambient pressure for an evaluation of the proposed concept.

$$CO_2 + 4\,H_2 \rightarrow CH_4 + 2\,H_2O \quad (1)$$

In general, the Sabatier reaction can be catalysed by transition metals such as Co [8,24–27], Ni [28–32], Ru [33–36], Rh [37] and to a very low extend by Pd [38,39]. Ni and Co are usually preferred over Ru and Rh due to the lower costs, but at the expense of lower activity. On the one hand on Co based catalysts, the reverse water gas shift reaction (2) takes place leading to decreased CH_4 selectivity.

$$CO_2 + H_2 \rightarrow CO + H_2O \quad (2)$$

On the other hand dissociative adsorption of CO_2 (3) typically takes place on free adsorption sites (*) on metallic cobalt surfaces [40].

$$CO_2 + 2^* \rightarrow CO^* + O^* \quad (3)$$

Hence, the dissociative CO_2 reaction path in combination with low binding strength of CO on cobalt additionally lead to a limited CH_4 selectivity.

In the CO_2 methanation reaction usually supported Co and Ni catalysts on Al_2O_3 [41,42], ZrO_2 [8,43], SiO_2 [44,45], TiO_2 [46,47], CeO_2 [48] and zeolites [30] are used. Co-based catalysts show relatively low selectivity towards methane and only a limited number of Co-based catalysts show suitable performances with high CO_2 conversion, high CH_4 selectivity and long catalyst lifetime. Conversions between 30% and 70% and CH_4 selectivity up to 90% are obtained on Co-based catalysts in a temperature range of 200–400 °C [21]. With Co/Al_2O_3 conversion rates of 75% and selectivity towards CH_4 of 80% are obtained at 270 °C if synthesized from nitrate precursors [11]. As described previously these Co/Al_2O_3 catalysts suffer from thermal degradation due to formation of an undesired $CoAl_2O_4$ spinel type secondary phase.

Theoretical studies suggest that metal support interaction play an important role for the activity and selectivity in CO_2 hydrogenation [49,50]. In general, activation of CO_2 can take place either on the metal surface, or on the surface of the support. Typically, the occurrence of CO adsorbed species from dissociative CO_2 adsorption indicates the activation on the metal surface, whereas carbonate and bicarbonate species relate on CO_2 activation on the support [40,51]. In both cases reaction mechanisms are proposed that react via CO or formate intermediates towards methane. The intermediate CO production by dissociative CO_2 adsorption on Co-based catalysts limits the obtained CH_4 selectivity [40]. Solely, for the direct CO_2 activation on the support a mechanism is proposed that excludes CO as an intermediate and reacts exclusively via formate [32,52–55]. This mechanism is proposed to take place on reducible supports (e.g. CeO_2 and ZrO_2) that enable spillover of hydrogen from the metal towards the surface of the support [32,55].

In the present study, the tailor ability of reduction behaviour of spinels is utilised and investigated how fractional changes of Mn in the Co-aluminate stoichiometry influence the catalytic performance in the CO_2 methanation as a test reaction. With extensive surface analysis by BET, H_2 and CO pulsed titration, CO_2-TPD and CO_2-DRIFTS it is analysed how the Mn incorporation alters these properties. Additional results from *operando* DRIFTS methanation experiments lead to conclusions for the observed improved catalytic performance of manganese modified catalysts precursor.

2. Experimental section

2.1. Catalyst preparation

$CoAl_{2-x}Mn_xO_4$ (x = 0, 0.1, 0.5, 1) catalysts were prepared by coprecipitation of the corresponding metal nitrates with NaOH. For this stoichiometric amounts according to the desired sum formula of $Co(NO_3)_2 \cdot 6H_2O$ (Sigma Aldrich, purity 98%), $Mn(NO_3)_3 \cdot 6H_2O$ (Sigma Aldrich, purity 98%) and $Al(NO_3)_3 \cdot 9H_2O$ (Sigma Aldrich, purity 98%) were dissolved in deionized water. The hydroxides precipitated by dropwise addition of 2 M aqueous NaOH under intense stirring until a pH of 10. The precipitate was filtered and washed with deionized water until neutrality. The obtained solids were dried for 8 h at 80 °C in a circulating air furnace and transferred into the oxides by calcination at 650 °C for 4 h (ramping 5 K/min) under a constant flow of air.

2.2. Characterization

X-Ray diffraction (XRD) of calcined and used catalysts were measured on a Bruker D8 Advance diffractometer with Ni filtered Cu K_α radiation (1.5406 Å) and a step size of 0.2° from 20 to 110°. Crystallite sizes (d_{cryst}) were calculated according the Debeye-Scherrer equation using the half width of the (3 1 1) reflex. Textural properties were determined by N_2-physisorption in a Quantachrome Autosorb IQ TPX. Prior to sorption measurements, the samples were degassed at 200 °C for 12 h in vacuum. Specific surface area (S_{BET}) was determined by the Brunauer-Emmett-Teller method at p/p_0 = 0.05–0.21.

Temperature-programmed analyses were performed on the same device in dynamic TPX mode. The samples were degassed for 30 min at 400 °C in a flow of N_2 (Pangas, 5.0) prior to the temperature-programmed reduction (TPR) analysis. TPR were performed in 5% H_2 in N_2 at a flow of 25 ml/min and a temperature ramp of 15 K/min to 900 °C. The change in gas composition was monitored by a thermal conductivity detector. For the temperature-programmed desorption of CO_2 (CO_2-TPD) a pre-reduction in H_2 (Pangas, 4.5) for 30 min at 500 °C, according to the pre-treatment conditions of catalytic screening, was performed. In such way, the number and strength of basic sites are comparable to the surface properties under reaction conditions. Remaining adsorbed H_2 was purged from the catalyst surface with He (Pangas, 4.6) for 30 min at 500 °C. After cooling down, pure CO_2 (Pangas, 4.8) was adsorbed at 100 °C for 30 min followed by

purging of physisorbed CO_2 for 30 min at 100 °C in He. CO_2-TPD were performed in a flow of 25 ml/min He and a ramping of 10 K/min to 600 °C.

Active metal surface areas were determined by CO (Pangas, 5.0) and H_2 pulsed titration after reduction of the samples at 500 °C for 30 min and purging at the same temperature with He for 2 h to desorb residual adsorbed H_2 from the surface. After cooling down to 40 °C in He, pulses of titration gas were injected by a calibrated sampling loop of the Quantachome Autosorb IQ TPX device. The pulses were injected in a flow of He until surface saturation. The apparent average metal particle sizes were calculated from the values of measured metal surface area via CO pulse titration assuming a M:CO stoichiometry of 1, a shape factor of 5 for spherical particles attached to the surface, and utilizing the corresponding uptake of hydrogen during pre-treatment to define the moles of metal contributing to the obtained metal surface area. The accuracy of procedure and measured adsorbed CO and H_2 amounts, were validated by the use of a Pt/Al_2O_3 standard, and yield in the same measured metals surface area for both titration gases. Elemental compositions of catalysts were measured by inductively-coupled-plasma-optic-emission-spectroscopy (ICP-OES) on an Agilent 720-ES device.

Diffuse reflectance infrared Fourier transform spectroscopy (DRIFTS) of adsorbed CO_2 species and *operando* analysis under methanation conditions were performed in a N_2 purged Bruker Vertex 70 infrared spectrometer equipped with a liquid N_2 cooled MCT detector. The sample compartment was equipped with a Harrick Praying Mantis DRIFTS chamber with a high temperature reaction cell and CaF_2 windows. The temperature was adjusted by a temperature controller and electrically heated. CO_2 adsorption-desorption experiments were performed in the DRIFTS gas cell to identify the nature of basic sites (Bønsted or Lewis) as a complementary analysis to CO_2-TPD. The catalysts were *in situ* reduced for 30 min at 550 °C in pure H_2 followed by a purging step with He for additional 30 min at 550 °C. After cooling down to 100 °C a background reference spectrum was collected in He. Then CO_2 was adsorbed until saturation at 100 °C and followed by purging with He at the same temperature to avoid the detection of physisorbed CO_2 species. CO_2 was desorbed in a flow of He and the temperature was increased stepwise starting from 200 to finally 500 °C. After 30 min of constant desorption temperature the sample was cooled down and equilibrated to 100 °C in a flow of He to collect the spectra (32 scans with a resolution of 2 cm^{-1}).

In the *operando* DRIFTS methanation experiments fresh catalysts were reduced in the reaction chamber like described previously. All background spectra of reduced materials were collected in a flow of He at the given temperature. At each temperature, first pure CO_2 was passed through the catalyst until saturation and no observable change of IR bands. Subsequently, it was switched to methanation conditions by changing the gas composition to CO_2 + H_2 with a stoichiometric ratio of 1:4. The change of surface species was continuously tracked and spectra were collected for about 20 min to obtain steady state conditions.

2.3. Catalytic performance

The activity of catalysts in the hydrogenation of CO_2 was measured using a fixed bed flow reactor (inner diameter 4 mm) at ambient pressure. In each test 200 mg of catalyst with a particle size of 250–400 μm filling a reactor volume of 0.21 ml was used. A pre-reduction of the catalyst for 30 min at 500 °C in a flow of H_2 was performed prior to the catalytic reaction in the reactor. Afterwards, CO_2 was added in a molar CO_2 to H_2 ratio of 1 to 4 at ambient pressure. Gas flows were adjusted by mass flow controller (Bronkhorst EL-Flow Select) to a total flow of 100 ml/min resulting in a GHSV of 28570 h^{-1}. During the catalytic run, the temperature was decreased from 500 °C to 200 °C in steps of 50 °C. Each temperature step was kept constant for 30 min in order to reach steady state conditions. Reactant and product gas compositions were continuously analysed online by a Kaiser Raman RXN2 spectrometer equipped with AirHead probes. The CO_2 conversion X, selectivity S to CH_4 and productivity were calculated according to Eqs. (3)–(5):

$$X(CO_2) = \frac{\dot{n}_{CO2,in} - \dot{n}_{CO2,out}}{\dot{n}_{CO2,in}} * 100\% \quad (3)$$

$$S(CH_4) = \frac{\dot{n}_{CH4,out}}{\dot{n}_{CO2,in} - \dot{n}_{CO2,out}} * 100\% \quad (4)$$

$$Productivity = \frac{\dot{n}_{CO2,in} - \dot{n}_{CO2,out}}{n_{catalyst}} \quad (5)$$

Wherein $\dot{n}_{CO2,in}$ and $\dot{n}_{CO2,out}$ represent the molar CO_2 concentration detected before and after the reactor, respectively. The produced molar concentration of CH_4 is represented by $\dot{n}_{CH4,out}$. $n_{catalyst}$ is the molar amount of Co within the reactor, irrespective if activated by reduction, or still present in the bulk of the catalyst. For each temperature step, the average of measured concentrations over the last 10 min of constant temperature was used for the calculations. Reported reaction rates in the Arrhenius plots where calculated under the condition of a reaction of pseudo first order, whereat the concentration of H_2 was kept much higher than the CO_2 concentration by maintaining the CO_2 conversion rate below 30%.

3. Results

3.1. Characterization of $CoAl_{2-x}Mn_xO_4$ precursor species

Phase analyses via XRD of spinels indicate the phase pure synthesis without detectable formation of secondary phases (cf. Fig. 1A). The shift in lattice parameter a_0 from 8.0988 to 8.2638 Å (cf. Table 1) as well as the change of reflex intensities (e.g. at 48.9° (1 3 3)-layer) according the occupation level of Mn proves the successful incorporation of Mn into the spinel in all compositions. All compositions show crystallite sizes in a comparable range between 28 and 38 nm and low specific surface areas of 3–33 m^2/g. The obtained type II isotherm indicates the absence of internal porosity for all catalysts. XRD of the catalysts after use in the CO_2 methanation reaction up to a temperature of 500 °C (Fig. 1b) shows that the spinel structure is completely retained for Mn amounts up to × = 0.5. Solely for $CoMnAlO_4$ the degradation products MnO (*) and Co (o) are observed next to the spinel phase. Based on the reflex position and applying Vegard's law this spinel has a composition of $CoMn_{0.747}Al_{1.252}O_4$. All other used catalyst show only a minor change in lattice parameter an hence similar Mn content after the catalytic run (Table 1). Hence, the spinel phase is stable under reaction conditions up to a Mn content of 0.75.

Temperature-programmed reduction analysis (TPR, Fig. 2) shows that incorporation of Mn in $CoAl_2O_4$ improves the reducibility and enables partial reduction of the material at temperatures lower than observed for $CoAl_2O_4$. As well, full reduction of the compounds shifted towards lower temperatures with increasing Mn content. The TPR can be distinguished in three sections. At temperatures between 200 and 450 °C reduction of Co^{2+} to Co^0 takes place [17,57]. In the same range Mn^{4+} reduces to Mn^{3+} (not present in the samples) and reduction of Mn^{3+} to Mn^{2+} is possible as well [58]. If Co^{2+} reduces to metallic Co^0 particles and is released from the spinel structure, then a portion of Mn^{3+} must be reduced to Mn^{2+} to stabilize the spinel structure by maintaining its charge neutrality. Bulk reduction of Co and Mn ($Mn^{3+}\rightarrow Mn^{2+}$) in

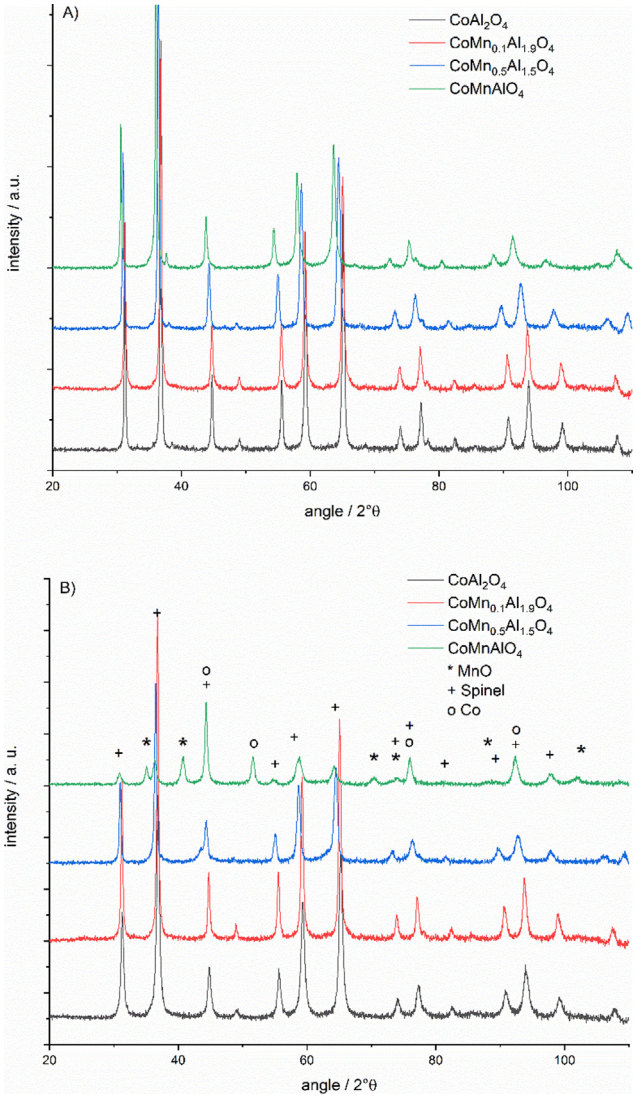

Fig. 1. XRD of (A) freshly synthesized $CoMn_xAl_{2-x}O_4$ and (B) reduced $CoMn_xAl_{2-x}O_4$ after the use as catalysts in the Sabatier reaction.

aluminates takes place at much higher temperature region (450–800 °C) due to the stabilizing effect of Al^{3+} by increasing the polarization of the Co-O bonds [57,59]. Complete reduction of Mn^{2+} to Mn^0 has been only observed at temperatures above 1000 °C [60]. Based on this discussion, the formation of metallic manganese during the applied pre-reduction of the catalysts is highly unlikely. From the shift of the bulk material reduction at high temperatures towards lower temperatures with increasing Mn quantity it is evident that the reduction capability of the spinels is increased by higher Mn quantities in the samples.

As well Ellingham diagrams [61] suggest the preferential reduction of Co over Mn in reductive environment. Even though the above discussion as well as thermodynamics suggest the preferential reduction of Co^{2+} towards metallic Co, it not possible at this stage to distinguish if Co, Mn or both metals are reduced. After reduction for 30 min in pure H_2 at 500 °C, according to the pretreatment conditions for catalytic testing, the measured active metal surface areas obtained from CO pulse titration are in the same range of 0.123–0.153 m^2/g for all tested catalysts (cf. Table 1). In line with these findings, the metal particles have similar apparent average particle diameter of 18–22 nm. Even though different particle size distributions might be present in the reduced catalysts the impact of the Co-particle size effect on the selectivity of the investigated catalysts is excluded on the basis of similar apparent average particle sizes. In contrast, measured metal surface areas obtained by H_2 are higher for the Mn modified spinels, while the unmodified spinel shows the same value as compared with the result from CO pulse titration (cf. Fig. 3). This behaviour points towards an enabled hydrogen spillover from the surface of the metal towards the oxide surface for the Mn modified catalysts only. The spillover is most pronounced for the $CoMn_{0.5}Al_{1.5}O_4$ precursor.

3.2. Catalytic performance of reduced $CoMn_xAl_{2-x}O_4$

The spinels with varying Mn content were used as catalysts in CO_2 methanation with H_2 at ambient pressure. Prior to the catalytic run, all catalyst precursor powders were exposed to a pre-reduction step for 30 min in pure H_2. Based on TPR analysis a moderate temperature of 500 °C was chosen in order to activate the oxide surface, but to prevent full reduction and thus preserving the spinel structure as the support. After pre-reduction a significant CO_2 conversion was observed for all compositions in the temperature range between 200 and 500 °C (Fig. 4A).

Compared to Mn-free $CoAl_2O_4$, all Mn incorporated spinels show substantially improved catalytic performance even though the accessible metal surface is the same in all catalysts (cf. Table 1). In order to rule out differences in Co loading due to differing spinel stoichiometry, the results are compared on the basis of productivity, whereat the obtained activity is normalized by the total number of moles Co included in the reactor of each composition, independent if Co is reduced or not. At 300 °C the catalyst productivity raises significantly by a factor of 24 from 0.025 for $CoAl_2O_4$ to 0.6 mol/(mol · min) for the most active composition of $CoMn_{0.5}Al_{1.5}O_4$. With the latter catalyst, having the highest productivity of 0.65 mol/(mol·min) at 400 °C. Also, the two remaining Mn containing compositions show substantial improved productivities compared to $CoAl_2O_4$, but the effect is less pronounced than for $CoMn_{0.5}Al_{1.5}O_4$. Additionally, Mn incorporation remarkably

Table 1
Calculated lattice parameter a_0 of calcined materials, determined crystallite size d_{cryst}, specific surface area S_{BET}, metal surface area (MSA) after reduction of investigated catalysts and average metal particle diameter d_{metal} obtained from CO-pulse titration, elemental composition obtained by ICP-OES, lattice parameter a_0 after use in the catalytic run and extracted Mn stoichiometry x within the $CoMn_xAl_{2-x}O_4$ according Vegard's law from lattice parameter of the used catalysts.

						Elemental Analysis			After use	
	a_0 (as calcined) /Å	d_{cryst} /nm	S_{BET} m^2/g	MSA m^2/g (CO)	d_{Metal}[1] /nm	Co wt%	Mn wt%	Al wt%	a_0 /Å	x[2]
$CoAl_2O_4$	8.09880(4)	38	15	0.123	21.5	33.3	0	30.5	8.09747(1)	0
$CoMn_{0.1}Al_{1.9}O_4$	8.10674(7)	30	33	0.165	18.4	32.8	3.1	28.5	8.10903(7)	0.083
$CoMn_{0.5}Al_{1.5}O_4$	8.18072(5)	28	9	0.143	19.6	30.9	14.4	21.2	8.17825(9)	0.493
$CoMnAlO_4$	8.26386(5)	36	3	0.153	18.7	28.8	26.8	13.2	8.22116(9)	0.747

[1] Calculated from CO-chemisorption: Values correspond to apparent average metal particle diameter.
[2] Calculated according to Vegard's law by the shift of lattice parameter.

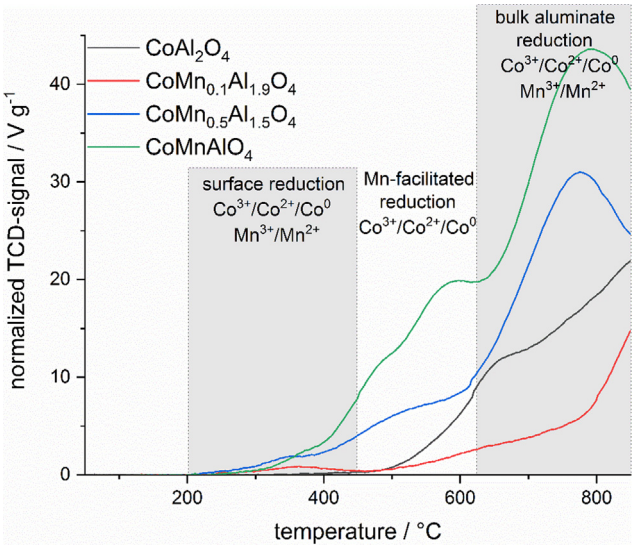

Fig. 2. TPR of calcined spinels with variation of stoichiometry.

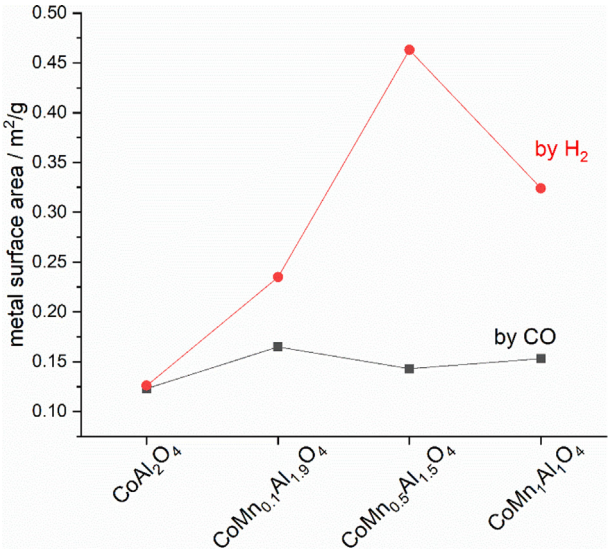

Fig. 3. Measured metal surface area after pre-reduction at 500 °C for 30 min for $CoMn_xAl_{2-x}O_4$ materials dependent on the titration gas CO vs H_2.

enhances the selectivity towards CH_4 in all compositions. In a wide range of temperatures from 300 to 450 °C the CH_4 selectivity of the most active catalyst $CoMn_{0.5}Al_{1.5}O_4$ is above 97%. In contrast, $CoAl_2O_4$ shows a rather low, but progressively increasing selectivity from 0 to 87% by increasing the temperature from 300 to 450 °C. In comparison to literature results on a Co/Al_2O_3 catalyst optimized with up to 0.43 wt% Pt [21] the herein presented $CoMn_{0.5}Al_{1.5}O_4$ catalyst shows 8% higher CO_2 conversion at 350 °C with comparable CH_4 selectivity under the same methanation conditions, but without the presence of any noble metal.

Extracted from Arrhenius-Plots (Fig. 5), the activation energy of CO_2 reduction to CH_4 drops from 108 kJ/mol on $CoAl_2O_4$ to 69 kJ/mol on $CoMn_{0.5}Al_{1.5}O_4$ (cf. Table 2). The activation energy of $CoAl_2O_4$ agrees well with literature data of 15 wt% Co/SiO_2 of 93 kJ/mol for Co systems on non-reducible supports [56]. The change of activation energy due to incorporation of Mn indicates a change of the catalytic active species or an alternative reaction mechanism, which will be discussed later. Catalysts with manganese content of $\times$ = 0.5 and 0.1 show a similar activation energy, indicating the presence of the same active sites and mechanism in those two compositions. The superior performance of $CoMn_{0.5}Al_{1.5}O_4$ over $CoMn_{0.1}Al_{1.9}O_4$ is explained by a higher number of active sites created by better dispersion and interaction between Co and Mn.

XRD analyses of the used catalysts indicate the stability of the catalysts by the presence of the spinel phase in all catalysts even after thermal treatment in reductive environment (cf. Fig. 1B).

Only in the XRD spectra of the $CoMnAlO_4$ catalyst, reflexes from MnO and Co appear as secondary phases after the catalytic run. This evidences the facilitated reducibility due to high Mn amounts incorporated in the structure. An excessively high reduction leads to destruction of the spinel phase and thus to lower catalytic activities.

3.3. Investigation of basic surface properties

In order to investigate changes of surface properties such as surface basicity, DRIFTS CO_2 adsorption-desorption measurements were performed to clarify the nature of basic sites on the surfaces of the catalysts (Fig. 6). On reduced $CoAl_2O_4$ (Fig. 6A) bands at 1674 and 1517 cm^{-1} belong to CO_2 adsorbed on surface OH-groups (weak basic sites) in form of a bicarbonate species [62]. Bands at 1618 and 1321 cm^{-1} are assigned to CO_2 adsorbed on Brønsted-acid-Lewis-basic pairs (medium basic sites) in a bidentate coordinating carbonate form [62]. Bands at 1563 and 1353 cm^{-1} indicate the presence of unidentate coordinating carbonate on strong basic

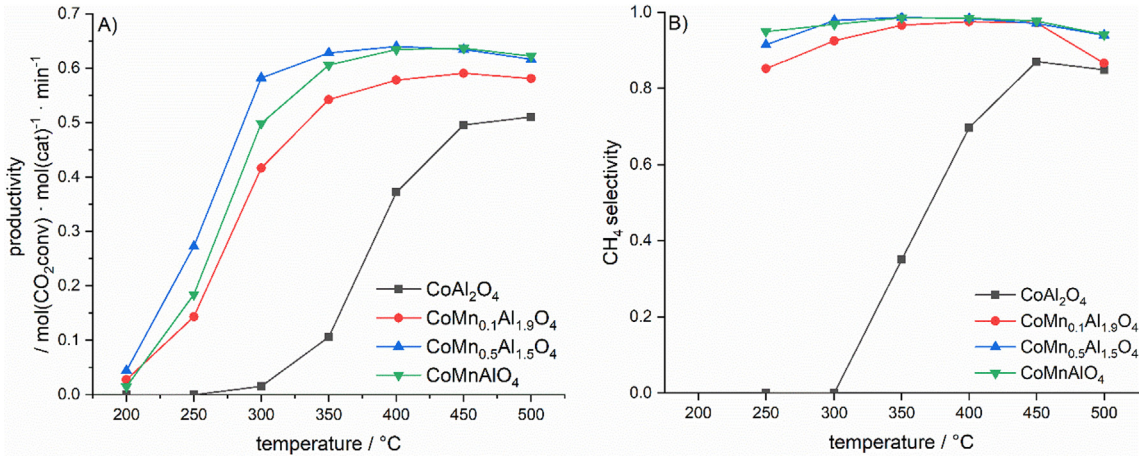

Fig. 4. Methanation performances of reduced catalysts. (A) Productivity of CO_2 conversions; (B) Selectivity towards CH_4. Reaction conditions: CO_2/H_2 = 1/4, $\dot{V}_{total}$ = 100 ml/min, GHSV = 28570 h^{-1}.

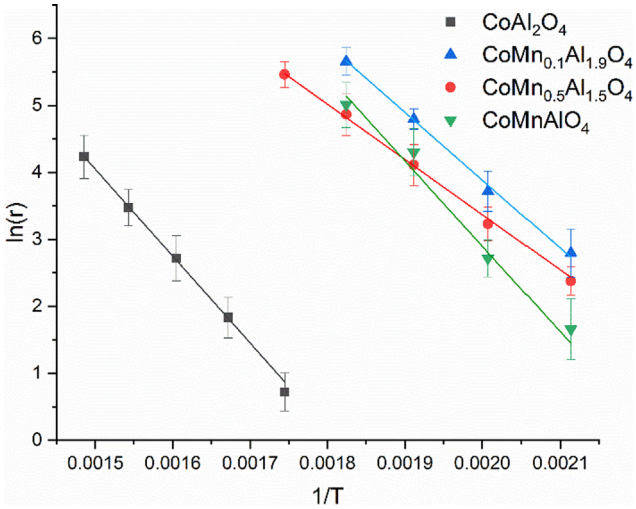

Fig. 5. Obtained Arrhenius-Plots for CO_2 hydrogenation of investigated reduced catalysts.

sites [62]. Desorption of CO_2 from the weak basic sites takes place between 100 and 200 °C. In the temperature region between 200 and 400 °C desorption of CO_2 from medium basic sites takes place while the intensity of bands from CO_2 adsorbed on strong basic sites remains constant over the screened temperature region. Because of amended electronic properties on reduced $CoMn_{0.5}Al_{1.5}O_4$ due to Mn incorporation, the position of bands of adsorbed CO_2 species are shifted (Fig. 6B). Bands of CO_2 on weak basic sites appear at 1647 and 1525 cm^{-1}, on medium basic sites at 1577 and 1291 cm^{-1} and on strong basic sites at 1553, 1403 and 1291 cm^{-1} [62]. The relative intensity of bands resulting from CO_2 adsorbed on weak basic sites is much lower than the intensity of medium and strong basic sites. This suggests a much higher relative concentration of medium and strong basic sites on the reduced $CoMn_{0.5}Al_{1.5}O_4$ as compared to reduced $CoAl_2O_4$. CO_2 desorption from weak basic sites takes place between 100 and 200 °C, from medium basic sites between 200 and 400 °C and bands of CO_2 adsorbed on strong basic sites still remain up to 500 °C.

TPD of CO_2 was conducted additionally to determine the desorption temperature of CO_2 and the number of weak, medium and strong basic sites (Fig. 7). Prior to the adsorption of CO_2 the samples were pre-reduced at 500 °C in pure H_2 for 30 min to analyse the surface properties as comparable as under reaction conditions.

The CO_2-TPD show that $CoAl_2O_4$ has a much higher number of basic sites than all other Mn containing spinels. The total number of basic sites decreases with increasing Mn content. Even a small Mn addition of × = 0.1 markedly decreases the total number of basic sites by a factor of 3.4 and 71% compared to $CoAl_2O_4$. This result clearly proves the strong impact of Mn on the basic surface properties of the herein investigated $CoAl_2O_4$ spinel. In all TPD measurements three different desorption peaks are deconvoluted and assigned to weak, medium and strong basic surface sites (cf. Table 2) according to CO_2-DRIFTS results. For spinels with × = 0.1 and 0.5 the desorption temperature of weak basic sites decreases slightly about 10 K. Especially the number of weak basic sites is significantly decreased by introduction of Mn into the spinel which is in agreement with the observed relative band intensities from CO_2-DRIFTS. In sum CO_2 desorption analysis shows a much higher degree of surface hydroxylation for reduced $CoAl_2O_4$ based catalysts in contrast to Mn incorporated reduced spinels. Hence, the improved selectivity of all Mn containing spinels correlates to the decreased number of weak basic sites and increased binding strength of CO_2 on the surface of the catalyst.

3.4. Operando DRIFTS CO_2-methanation investigations

In order to understand the increased activity and selectivity due to Mn integration into the spinel, *operando* DRIFTS measurements were performed under CO_2 methanation conditions as a function of reaction temperature (Fig. 8). In order to distinguish between adsorbed CO_2 species and hydrogenated reaction intermediates, only CO_2 was initially introduced into the reaction chamber until all signals had stabilized. Subsequently, H_2 was added at to the CO_2 flow, resulting in a CO_2:H_2 ratio of 1:4, until no further change in signals was observed.

Under continuous CO_2 feed (dotted lines in Fig. 8) bands of weakly bonded bicarbonate species or physisorbed CO_2 at 1674 and 1517 cm^{-1} appear at 100 °C on reduced $CoAl_2O_4$. These bands decrease in intensity with increasing temperature on reduced $CoAl_2O_4$ (Fig. 8A) while a small shoulder stays present even at elevated temperatures up to 500 °C. Additionally, bands from bidentate coordinating carbonate at 1624 and 1320 cm^{-1} and unidentate coordinating carbonate at 1559 and 1365 cm^{-1} appear at all temperatures [62]. Especially at 100 °C, but also up to 250 °C a broad band of adsorbed CO [63] between 2000 and 2200 cm^{-1} is visible. The broadness originates from the superposition of CO adsorption in different geometries (linear CO-Co^0 at 2059 cm^{-1} and bridged CO-Co^0 at 1942 cm^{-1}) as well as different Co sites present within the catalysts (CO-Co^{+2} at 2176 cm^{-1} and CO-Co^{1+} at 2143 cm^{-1}) [64]. The appearance of CO upon CO_2 adsorption indicates a dissociative adsorption on the surface of the catalyst. In line with the appearance of CO surface species and increase of reaction temperature CO is detected as a reaction product in the gas phase. Under continuous CO_2 and H_2 feed (solid lines in Fig. 8) no significant changes of adsorbed species or relative intensities compared to H_2 free conditions are present on the reduced $CoAl_2O_4$ catalyst. Solely at 500 °C the intensity of bands related to bidentate coordinating carbonate species at medium basic sites decrease slightly upon H_2 addition. CO is the only observed reaction intermediate at all reaction temperatures.

In the case of reduced $CoMn_{0.5}Al_{1.5}O_4$ catalyst in pure CO_2 (dotted lines in Fig. 8B) bands from physisorbed or weakly adsorbed bicarbonate species (1647 and 1220 cm^{-1}) [62] are present at 100 °C. Bands from this species completely vanish indicating no significant CO_2 adsorption on weak basic sites at temperatures higher than 250 °C. Above this temperature and in pure CO_2 atmosphere, bi- and unidentate coordinating carbonates are the main adsorbed species on medium and strong basic sites respectively. In addition, the absence of any detectable CO bands shows that

Table 2
Obtained activation energies (E_A), molar amount of desorbed CO_2 $n(CO_2)_{des}$, amount of weak (n_{weak}), medium (n_{medium}) and strong (n_{strong}) basic sites derived from CO_2-TPD.

	E_A kJ/mol	$n(CO_2)_{des}$ µmol/g	n_{weak} µmol/g	n_{medium} µmol/g	n_{strong} µmol/g
$CoAl_2O_4$◦	108 (±2)	111.98	34.73	41.20	36.05
$CoMn_{0.1}Al_{1.9}O_4$	84 (±3)	32.77	10.35	9.83	12.59
$CoMn_{0.5}Al_{1.5}O_4$	69 (±2)	15.59	2.61	6.48	6.50
$CoMnAlO_4$	106 (±12)	6.00	1.15	3.97	0.87

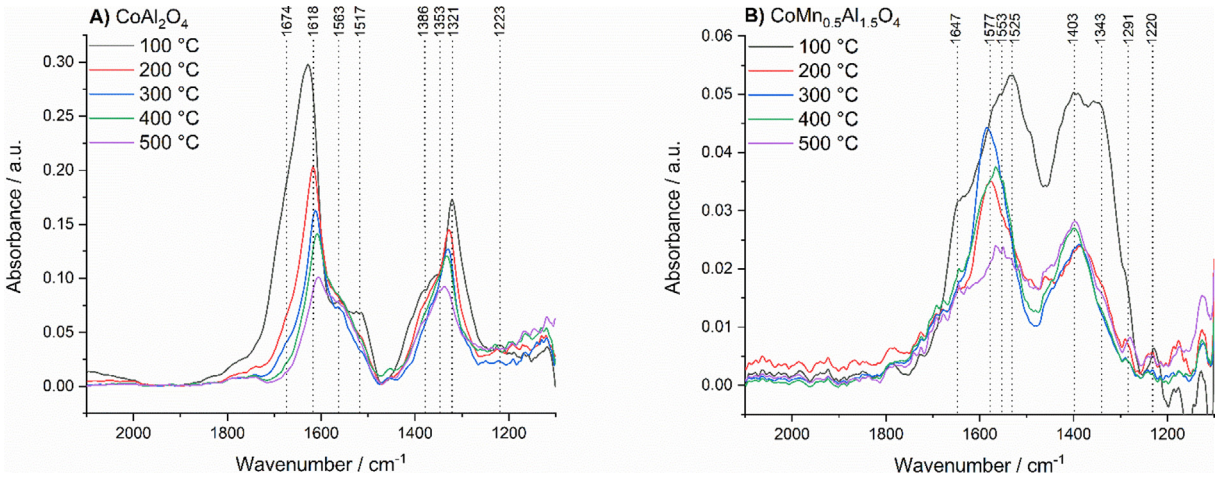

Fig. 6. DRIFTS analysis of stability of adsorbed CO_2 species for the identification of surface basicity of A) $CoAl_2O_4$ and B) $CoMn_{0.5}Al_{1.5}O_4$.

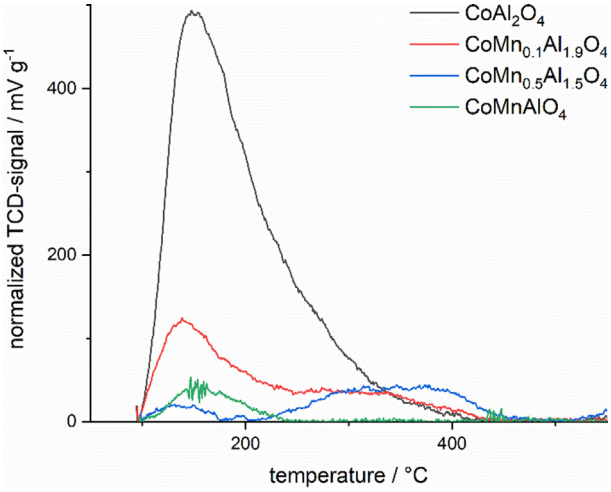

Fig. 7. TPD of CO_2 on reduced catalysts with different compositions.

CO_2 is not dissociatively adsorbed on the surface of Co-metal but preferentially adsorbed on the surface of the oxide. After changing from pure CO_2 to stoichiometric methanation conditions significant changes appear in the DRIFTS spectra at temperatures above 150 °C: Bands resulting from adsorbed formate species appear at 1585 and 1368 cm^{-1}. The appearance of this species correlates to the observed increasing catalytic activity. Compared to literature values [65] the position of these two bands shift due to superposition of bands originating from formate (1598 cm^{-1}; 1372 cm^{-1}) and unidentate carbonates species (1577 and 1353 cm^{-1}). Additionally, a shoulder at 1313 cm^{-1} appears at 250 °C and higher temperatures showing the formation of methane [65,66]. Neither in pure CO_2 nor under methanation conditions do bands appear in the spectra that indicate the presence of CO-species on the surface of the reduced $CoMn_{0.5}Al_{1.5}O_4$ catalyst. The absence of a dissociative CO_2 adsorption by formation of CO surface intermediates indicates a shift of CO_2 activation from the Co metal surface onto the surface of the support itself.

4. Discussion of improved reactivity

As shown by TPR and CO_2-adsorption experiments (DRIFTS and CO_2-TPD), introduction of manganese into the crystal structure alters the surface properties. This leads to an improved catalytic performance and a lower activation energy for CO_2 methanation from 108 to 69 kJ/mol on the reduced $CoMn_{0.5}Al_{1.5}O_4$ catalyst compared to the reduced $CoAl_2O_4$ catalyst. All catalysts possess bifunctional character upon reduction: metallic sites enable dissociation of H_2 and the oxidic support adsorption of CO_2. The observed difference induced by Mn incorporation and its effect on CO_2 hydrogenation towards CH_4 is discussed in the following:

$CoAl_2O_4$ shows the lowest reducibility of all analysed mixed-metal oxides. Nevertheless, Co reduces from the spinel and forms metal particles on the surface with comparable average metal particle diameter as in the Mn incorporated case. Due to the relatively high temperatures necessary to detect significant reduction of the bulk (TPR), the surface of the support has manly non-reductive character at reaction temperatures relevant for CO_2 methanation and thus does not enable hydrogen spillover from the metal centre towards the oxide surface. Additionally, after pre-reduction the support surface of reduced $CoAl_2O_4$ is in a highly hydroxylated state as evidenced by CO_2-adsorption experiments (TPD & DRIFTS). CO_2 adsorbs preferentially as bicarbonate species upon reaction with the weak basic surface hydrogen groups on highly hydroxylated surfaces [67]. Even without presence of H_2, dissociative CO_2 adsorption into adsorbed CO and O species takes place on the metallic Co sites. This is evidenced by the presence of CO species from DRIFTS-CO_2 desorption experiments. These adsorbed CO species fully desorb until 250 °C, indicating a weak bonding of CO with the surface of the catalyst and providing the reason for the low selectivity towards methane. The only observed reaction intermediate at all temperatures is CO within *operando* DRIFTS methanation experiments. Only at 500 °C a decrease of surface bicarbonate species is visible upon change of reaction conditions from pure CO_2 to a mixture of H_2 and CO_2. The production of CH_4 starts already at 350 °C. The decrease of bands originate from bicarbonate species only at much higher temperatures than necessary to produce CH_4 and this indicates the preferential adsorption of this species on the support. Hence, conversion of the bicarbonate species becomes considerable only at very high temperatures. Based on these observations, CO_2 methanation on reduced $CoAl_2O_4$ proceed similar to Co/Al_2O_3. The observed characteristics correspond to literature results suggesting activation of H_2 as well as CO_2 conversion on the surface of the Co-nanoparticles via CO as the main reaction intermediate [40]. The low CH_4 selectivity is the result of the low bond strength of CO on the surface and the preferential CO desorption at lower reaction temperature. Only at elevated temperatures, hydrogenation of CO becomes fast enough to produce significant amounts of CH_4. For this reason, reduced $CoAl_2O_4$ has a high selectivity to CO below 450 °C. This conclusion

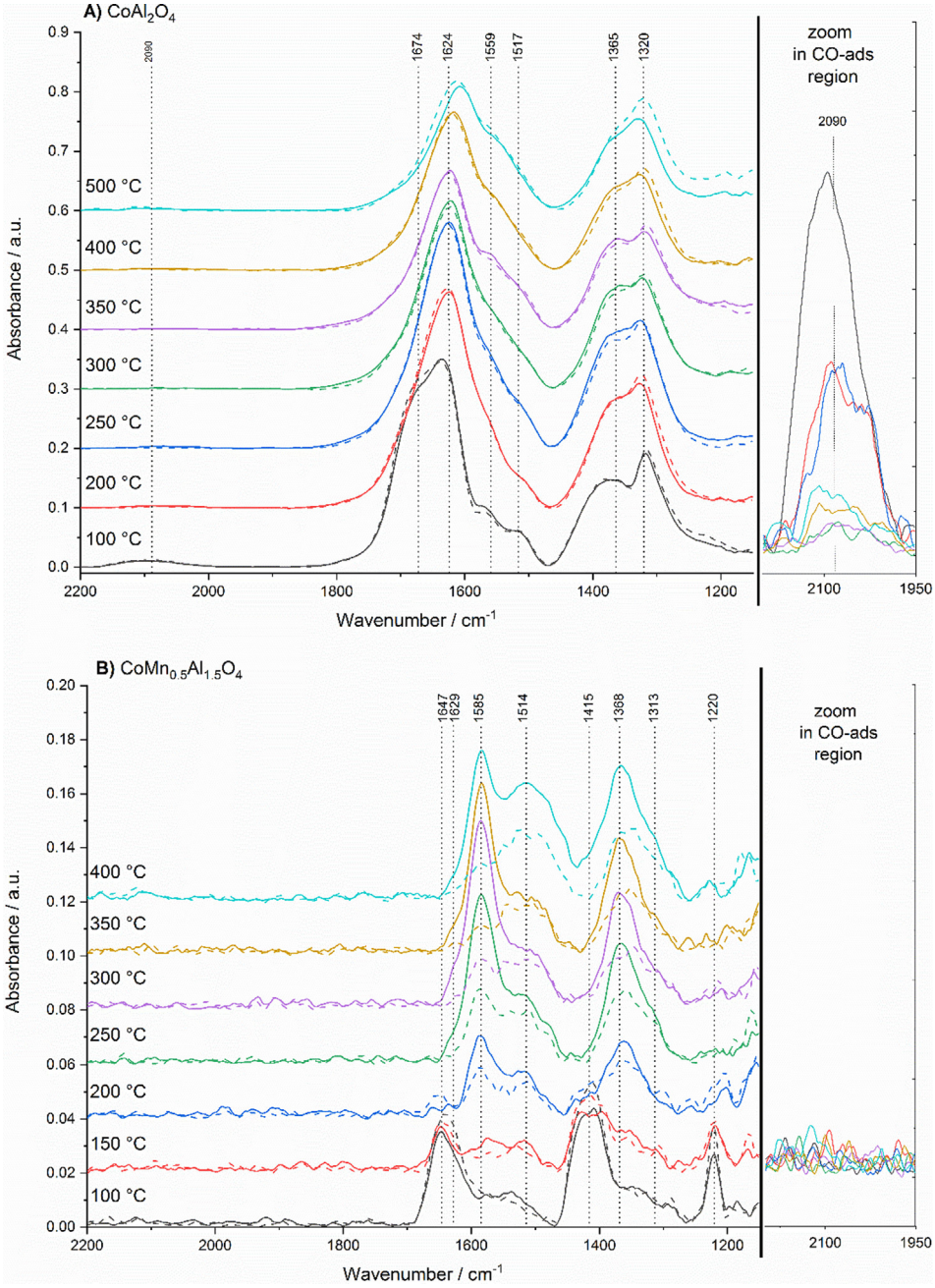

Fig. 8. *Operando* DRIFTS analysis after CO_2 adsorption (dotted lines) and under methanation conditions (solid lines) at indicated temperatures and zoom into the CO-adsorbed region. (A) $CoAl_2O_4$; B) $CoMn_{0.5}Al_{1.5}O_4$. Reaction conditions: Pre-reduction at 500 °C in H_2 for 30 min and purging in He, CO_2 adsorption in pure CO_2 until saturation, addition of H_2 with CO_2:H_2 = 1:4.

is in line with the proposed reaction mechanism of CO_2 methanation on supported Co on non-reducible supports.

In contrast, reduced $CoMn_{0.5}Al_{1.5}O_4$ shows a much lower total number of basic sites. But the available sites have a stronger basicity. Hence, this material has a less hydroxylated surface. As shown in DRIFTS experiments, CO_2 adsorbs as carbonate species upon reaction with the stronger basic surface oxygen sites of reduced $CoMn_{0.5}Al_{1.5}O_4$. Evidenced by the high desorption temperature in CO_2-TPD, these carbonate species have a much higher binding strength with the surface of the catalyst compared to the binding strength of bicarbonate species on reduced $CoAl_2O_4$. In conclusion: From the absence of adsorbed CO intermediates formed in DRIFTS experiments, CO_2 does not adsorb predominantly in a dissociative way on $CoMn_{0.5}Al_{1.5}O_4$. Instead, bands originating from formate species rise in the *operando* DRIFTS-spectra upon H_2 addition. Due to the reducible character of the oxide surface under methanation conditions and evidenced by pulse titration experiments, hydrogen spillover from the Co particles towards the surface of the Mn modified oxides is enabled most likely via the Mn^{3+}/Mn^{2+} redox couple. Consequently, conversion of CO_2 on the surface of the oxide support becomes possible. The reaction of hydrogen with the carbonate species on the surface of the oxide stands in line with the observed strong signals of formate species detected in *operando* DRIFTS methanation experiments. Due to the strong intensity of these bands the signals cannot solely originate from species adsorbed on the metal surface. Hence, the surface of the support gets involved in the catalytic reaction. In addition, all observed characteristics point towards a reaction mechanism that

is comparable to CeO_2, ZrO_2 or CeO_2-ZrO_2 supported systems via formate intermediates [32,52–55]. Hence, the observed significant improvement of the catalytic activity towards CO_2 methanation of Mn integrated systems can be understood by a shift of CO_2 methanation from the surface of the metal nanoparticles towards the surface of the support. In addition, CO_2 hydrogenation is enabled on the support via a reaction path mediated by formates. In the case of reduced $CoAl_2O_4$ the support is non-reducible at reaction temperatures. Hence, it is not capable of enabling hydrogen spillover from the metal centre towards adsorbed CO_2 on the support. The only remaining reaction site is the surface of the Co-nanoparticles itself under preferential CO formation or the interstitial area between the metal nanoparticle and its support. Whereas the whole surface of reduced Mn modified catalysts is utilised as catalytic active surface area. Hence, the improved reducibility of the oxide is the key factor to shift the reaction from the metal nanoparticle towards the surface of the support and subsequently leading to substantially higher active surface area.

5. Conclusions

The herein presented results show, that the use of spinel based solid solutions are suited to be used as catalyst precursor species for Co based methanation catalysts, even though $CoAl_2O_4$ is in general detrimental for this reaction. In order to obtain best methanation activity the spinel phase is additionally modified in reducibility by the introduction of manganese species into the structure and the reducibility depends on the Mn content within the structure. The most suited solid solution precursor composition for CO_2 methanation within this study is $CoMn_{0.5}Al_{1.5}O_4$ pre-reduced at 500 °C. Compared to the pure $CoAl_2O_4$ precursor the number of weak basic sites decreases, while the bond strength with CO_2 increases by modification of the spinel with Mn after pre-reduction. In addition, hydrogen spillover from the active Co sites towards the spinel support is enabled due to Mn incorporation. These modifications yield into a significantly improved catalytic performance on the Mn incorporated catalysts. This is accompanied by drastically lowered activation energy from 108 kJ/mol to 69 kJ/mol. Therefore, this work emphasizes, if Mn is present in the spinel the reaction site shifts from the Co metal surface solely via a CO-mediated reaction path towards the surface of the support via a formate-mediated reaction mechanism. On the Mn modified spinel precursor, the dissociative CO_2 adsorption of cobalt-based catalysts is suppressed. Hence, formation of CO as a by-product in CO_2 methanation is decreased. Besides, the enabled hydrogen spillover facilitates CO_2 hydrogenation on the surface of the support as well. This results into a significantly increased catalytic active surface area of the Mn modified catalysts in contrast to the limited active metal surface area of the unmodified catalyst.

Declaration of Competing Interest

The authors declare that they have no known competing financial interests or personal relationships that could have appeared to influence the work reported in this paper.

Acknowledgements

The authors kindly acknowledge the funding of SMARTCAT (grant number: SI/501130-01) by the Swiss Federal Office of Energy. The authors are grateful for the financial support provided by the Swiss National Science Foundation (SNSF) within the National Research Programme "Energy Turnaround" (NRP 70). Further information on the National Research Programme can be found at www.nrp70.ch.

References

[1] B. Kahn, Earth's CO_2 passes the 400 ppm threshold – maybe permanently, Climate Central (2016).
[2] J. Baier, G. Schneider, A. Heel, A cost estimation for CO_2 reduction and reuse by methanation from cement industry sources in Switzerland, Front. Energy Res. 6 (2018), https://doi.org/10.3389/fenrg.2018.00005.
[3] W. Li, H. Wang, X. Jiang, J. Zhu, Z. Liu, X. Guo, C. Song, A short review of recent advances in CO_2 hydrogenation to hydrocarbons over heterogeneous catalysts, RCS Adv. 8 (2018) 7651–7669, https://doi.org/10.1039/C7RA13546G.
[4] M. Specht, J. Brellochs, V. Frick, B. Stürmer, U. Zuberbühler, M. Sterner, G. Waldstein, Storage of renewable energy in the natural gas grid, ERDÖL ERDGAS KOHLE 126 (2010) 342–346.
[5] M. Bailera, P. Lisbona, L.M. Romeo, S. Espatolero, Power to gas project review: lab, pilot and demo plants for storing renewable energy and CO_2, Renew. Sustain. Energy Rev. 69 (2017) 292–312, https://doi.org/10.1016/j.rser.2016.11.130.
[6] Y. Yao, X. Li, D. Hildebrandt, D. Glasser, The effect of CO_2 on a cobalt-based catalyst for low temperature Fischer-Tropsch synthesis, Chem. Eng. J. 193–194 (2012) 318–327, https://doi.org/10.1016/j.cej.2012.04.045.
[7] C.G. Visconti, L. Lietti, E. Tronconi, P. Forzatti, R. Zennaro, E. Finocchio, Fischer-Tropsch synthesis on a Co/Al_2O_3 catalyst with CO_2 containing syngas, Appl. Catal. A 355 (2009) 61–68, https://doi.org/10.1016/j.apcata.2008.11.027.
[8] W. Li, X. Nie, X. Jiang, A. Zhang, F. Ding, M. Liu, Z. Liu, X. Guo, C. Song, ZrO_2 support imparts superior activity and stability of Co catalysts for CO_2 methanation, Appl. Catal. B 220 (2018) 397–408, https://doi.org/10.1016/j.apcatb.2017.08.048.
[9] J. Zhang, J. Chen, J. Ren, Y. Sun, Chemical treatment of γ-Al_2O_3 and its influence on the properties of Co-based catalysts for Fischer-Tropsch synthesis, Appl. Catal. A 243 (2003) 121–133, https://doi.org/10.1016/S0926-860X(02)00541-0.
[10] B. Jongsomjit, J. Panpranot, J.G. Goodwin Jr., Co-support compound formation in alumina-supported cobalt catalysts, J. Catal. 204 (2001) 98–109, https://doi.org/10.1006/jcat.2001.3387.
[11] N. Srisawad, W. Chaitree, O. Mekasuwandumrong, A. Shotipruk, B. Jongsomjit, J. Panpranot, CO_2 hydrogenation over Co/Al_2O_3 catalysts prepared via a solid-state reaction of fine gibbsite and cobalt precursors, React. Kinet. Mech. Catal. 107 (2012) 179–188, https://doi.org/10.1007/s11144-012-0459-8.
[12] W.J. Wang, Y.W. Chen, Influence of metal loading on the reducibility and hydrogenation activity of cobalt/alumina catalysts, Appl. Catal. 77 (1991) 223–233, https://doi.org/10.1016/0166-9834(91)80067-7.
[13] R.L. Chin, D.M. Hercules, Surface spectroscopic characterization of cobalt-alumina catalysts, J. Phys. Chem. 86 (1982) 360–367, https://doi.org/10.1021/j100392a016.
[14] M.-M. Millet, A.V. Tarasov, F. Girgsdies, G. Algara-Siller, R. Schlögl, E. Frei, Highly dispersed $Ni^0/Ni_xMg_{1-x}O$ catalysts derived from solid solutions: how metal and support control the CO_2 hydrogenation, ACS Catal. 9 (2019) 8534–8546, https://doi.org/10.1021/acscatal9b02332.
[15] D. Papargyriou, D.N. Miller, J.T. Irvine, Exsolution of Fe-Ni alloy nanoparticles from (La, Sr)(Cr, Fe, N_i)O3 perovskites as potential oxygen transport membrane catalysts for methane reforming, J. Mater. Chem. A 7 (2019) 15812–15822, https://doi.org/10.1039/c9ta03711j.
[16] P. Steiger, R. Delmelle, D. Foppiano, L. Holzer, A. Heel, M. Nachtegaal, O. Kröcher, D. Ferri, Structural reversibility and nickel particle stability in lanthanum iron nickel perovskite-type catalysts, ChemSusChem 10 (11) (2017) 2505–2517, https://doi.org/10.1002/cssc.201700358.
[17] T. Franken, R. Palkovits, Investigation of potassium doped mixed spinels $Cu_xCo_{3-x}O_4$ as catalyst for an efficient N_2O decomposition in real reaction conditions, Appl. Catal. B 176–177 (2015) 298–305, https://doi.org/10.1016/j.apcatb.2015.04.002.
[18] N. Bahlawane, P.H.T. Ngamou, V. Vannier, T. Kottke, J. Heberle, K. Kohse-Höinghaus, Tailoring the properties and the reactivity of the spinel cobalt oxide, Phys. Chem. Chem. Phys. 11 (2009) 9224–9232, https://doi.org/10.1039/B910707J.
[19] J.B. Goodenough, A.L. Loeb, Theory and ionic ordering, crystal distortion, and magnetic exchange due to covalent forces in spinels, Phys. Rev. 98 (1955) 391–408, https://doi.org/10.1103/PhysRev. 98.391.
[20] S.M. Antao, L.A. Cruickshank, K.S. Hazrah, Structural trends and solid-solutions based on the crystal chemistry of two hausmannite (Mn_3O_4) samples from the Kalahari Manganese Field, Minerals 9 (2019) 343–359, https://doi.org/10.3390/min9060343.
[21] M. Schubert, S. Pokhrel, A. Thomé, V. Zielsek, T.M. Gesing, F. Roessner, L. Mädler, M. Bäumer, Highly active Co-Al_2O_3-based catalysts for CO_2 methanation with very low platinum promotion prepared by double flame spray pyrolysis, Catal. Sci. Technol. 6 (2016) 7449–7460, https://doi.org/10.1039/C6CY01252C.
[22] F. Morales, B.W. Weckhuysen, Promotion effects in Co-based Fischer-Tropsch catalysis, Catalysis 19 (2006) 1–40, https://doi.org/10.1039/9781847555229-00001.
[23] M. Minnermann, S. Pokhrel, K-. Thiel, R. Henkel, J. Birkenstock, T. Laurus, A. Zargham, J.-I. Flege, V. Zielasek, E. Piskorska-Hommel, J. Falta, L. Mädler, M. Bäumer, Role of palladium in iron based Fischer-Tropsch catalysts prepared by flame spray pyrolysis, J. Phys. Chem. C 115 (2011) 1302–1310, https://doi.org/10.1021/jp106860d.

[24] J. Janlamool, P. Praserthdam, B. Jongsomjit, Ti-Si composite oxide-supported catalysts for CO_2 hydrogenation, J. Nat. Gas. Chem. 20 (2011) 558–564, https://doi.org/10.1016/S1003-9953(10)60213-7.
[25] Z. Guilin, W. Tian, X. Hongmei, Z. Xuxu, Effects of structure on the carbon dioxide methanation performance of Co-based catalysts, Int. J. Hydrogen Energy 38 (2013) 10012–10018, https://doi.org/10.1016/j.ijhydene.2013.05.130.
[26] G.L. Zhou, T. Wu, H.B. Zhang, H.M. Xie, Y.C. Feng, Carbon dioxide methanation on ordered mesoporous Co/KIT-6 catalysts, Chem. Eng. Commun. 201 (2014) 233–240, https://doi.org/10.1080/00986445.2013.766881.
[27] H.H. Shin, L. Lu, Z. Yang, C.J. Kiely, S. McIntosh, Cobalt catalysts decorated with platinum atoms supported on barium zirconate provide enhanced activity and selectivity for CO_2 methanation, ACS Catal. 6 (2016) 2811–2818, https://doi.org/10.1021/acscatal.6b00005.
[28] G. Du, S. Lim, Y. Yang, C. Wang, L. Pfefferle, G.L. Haller, Methanation of carbon dioxide on Ni-incorporated MCM-41 catalysts: the influence of catalyst pretreatment and study of steady-state, J. Catal. 249 (2007) 370–379, https://doi.org/10.1016/j.jcat.2007.03.029.
[29] I. Rossetti, C. Biffi, C.L. Bianchi, V. Nichele, M. Signoretto, F. Menegazzo, E. Finocchio, G. Ramis, A. Di Micele, Ni/SiO_2 and Ni/ZrO_2 catalysts for the steam reforming of ethanol, Appl. Catal. B 117–118 (2012) 384–396, https://doi.org/10.1016/j.apcatb.2012.02.006.
[30] R. Delmelle, R.B. Duarte, T. Franken, D. Burnat, L. Holzer, A. Borgschulte, A. Heel, Development of improved nickel catalysts for sorption enhanced CO_2 methanation, Int. J. Hydrogen Energy 41 (2016) 20185–20191, https://doi.org/10.1016/j.ijhydene.2016.09.045.
[31] A. Vita, C. Italiano, L. Pino, P. Frontera, M. Ferraro, Activity and stability of powder and monolith-coated Ni/GDC catalysts for CO_2 methanation, Appl. Catal. B 226 (2018) 384–395, https://doi.org/10.1016/j.apcatb.2017.12.078.
[32] A. Solis-Garcia, J.F. Louvier-Hernandez, A. Almendarez-Camarillo, J.C. Fierro-Gonzales, Participation of surface bicarbonate, formate and emthoxy species in the carbon dioxide methanation catalysted by ZrO_2-supported Ni, Appl. Catal. B 218 (2017) 611–620, https://doi.org/10.1016/j.apcatb.2017.06.063.
[33] D. Theleritis, S. Souentie, A. Siokou, A. Katsaounis, C.G. Vayenas, Hydrogenation of CO2 over Ru/YSZ electropromoted catalysts, ACS Catal. 2 (2012) 770–780, https://doi.org/10.1021/cs300072a.
[34] J.H. Kwak, L. Kovarik, J. Szanyi, CO_2 reduction on supported Ru/Al_2O_3 catalysts: cluster size dependence of product selectivity, ACS Catal. 3 (2013) 2449–2455, https://doi.org/10.1021/cs400381f.
[35] A. Petala, P. Panagiotopoulou, Methanation of CO_2 over alkali-promoted Ru/TiO_2 catalysts: I. Effect of alkali additives on catalytic activity and selectivity, Appl. Catal. B 224 (2018) 919–927, https://doi.org/10.1016/j.apcatb.2017.11.048.
[36] L. Falbo, M. Mertinelli, C.G. Visconti, L. Lietti, C. Bassano, P. Deiana, Kinetics of CO_2 methanation on a Ru-based catalyst at process conditions relevant for Power-to-Gas applications, Appl. Catal. B 225 (2018) 354–363, https://doi.org/10.1016/j.apcatb.2017.11.066.
[37] A. Karelovic, P. Ruiz, CO_2 hydrogenation at low temperature over Rh/γ-Al_2O_3 catalysts: effect of the particle size on catalytic performances and reaction mechanism, Appl. Catal. B 113–114 (2012) 237–249, https://doi.org/10.1016/j.apcatb.2011.11.043.
[38] J.N. Park, E.W. McFarland, A highly dispersed Pd-Mg/SiO_2 catalyst active for methanation of CO_2, J. Catal. 266 (2009) 92–97, https://doi.org/10.1016/j.jcat.2009.05.018.
[39] J.H. Kwak, L. Kovarik, J. Szanyi, Heterogeneous catalysis on atomically dispersed supported metals: CO_2 reduction on multifunctional Pd catalysts, ACS Catal. 3 (2013) 2094–2100, https://doi.org/10.1021/cs4001392.
[40] A. Solis-Garcia, J.C. Fierro-Gonzalez, Mechanistic insights into the CO_2 methanation catalyzed by supported metals: a review, J. Nanosci. Nanotechnol. 19 (2019) 3110–3123, https://doi.org/10.1166/jnn.2019.16606.
[41] R. Razzaq, C. Li, M. Usman, K. Suzuki, S. Zhang, A highly active and stable Co_4N/γ-Al_2O_3 catalyst for CO and CO_2 methanation to produce synthetic natural gas (SNG), Chem. Eng. J. 262 (2015) 1090–1098, https://doi.org/10.1016/j.cej.2014.10.073.
[42] J. Liu, D. Cui, J. Yu, F. Su, G. Xu, Performance characteristics of fluidized bed syngas methanation over Ni-Mg/Al_2O_3, Chinese J. Chem. Eng. 23 (2015) 86–92, https://doi.org/10.1016/j.cjche.2014.09.038.
[43] G.R. Johnson, A.T. Bell, Role of ZrO_2 in promoting the activity and selectivity of Co-based Fischer-Tropsch synthesis catalysts, ACS Catal. 6 (2016) 100–114, https://doi.org/10.1021/acscatal.5b02205.
[44] M.A.A. Aziz, A.A. Jalil, S. Triwahyono, R.R. Mukti, Y.H. Taufiq-Yap, M.R. Sazegar, Highly active Ni-promoted mesostructured silica nanoparticles for CO_2 methanation, Appl. Catal. B 147 (2014) 359–368, https://doi.org/10.1016/j.apcatb.2013.09.015.
[45] Z.Q. Wang, Z.N. Xu, S.Y. Peng, M.J. Zhang, G. Lu, Q.S. Chen, Y. Chen, G.C. Guo, High-performance and long-lived Cu/SiO_2 nanocatalysts for CO_2 hydrogenation, ACS Catal. 5 (2015) 4255–4259, https://doi.org/10.1021/acscatal.5b00682.
[46] G. Zheng, J. Qiu, Z. Li, P. Pavaskar, S.B. Cronin, CO_2 reduction to methanol on TiO_2-passicated GaP photocatalysts, ACS Catal. 4 (2014) 3512–3516, https://doi.org/10.1021/cs500697w.
[47] N. Shimoda, D. Shoji, K. Tani, M. Fujiwara, K. Urasaki, R. Kikuchi, S. Satokawa, Role of trace chlorine in Ni/TiO_2 catalysts for CO selective methanation in reformate gas, Appl. Catal. B 174 (2015) 486–495, https://doi.org/10.1016/j.apcatb.2015.03.026.
[48] F. Wang, C. Li, X. Zhang, M. Wei, D.G. Evans, X. Duan, Catalytic behavior of supported Ru nanopartces on the 1 0 0}, {1 1 0}, and {1 1 1 facet of CeO2, J. Catal. 329 (2015) 177–186, https://doi.org/10.1016/j.jcat.2015.05.014.
[49] K. Lamier, W.C. Liao, S. Tada, E. Lam, R. Verel, A. Bansode, A. Urakawa, A. Comas-Vives, C. Copéret, CO_2-to-methanol hydrogenation on zirconia-supported copper nanoparticles: reaction intermediates ant the role of the metal-support-interface, Angew. Chem. Int. Ed. 56 (2017) 2318–2323, https://doi.org/10.1002/anie.201610166.
[50] M.-C. Silaghi, A. Comas-Vives, C. Copèret, CO_2 activation on Ni/γ-Al_2O_3 catalysts by first-principles calculations: from ideal surfaces to supported nanoparticles, ACS Catal. 6 (2016) 4501–4505, https://doi.org/10.1021/acscatal.6b00822.
[51] C. Vogt, M. Monai, G.J. Kramer, B.M. Weckhuysen, The renaissance of the Sabatier reaction and its applications on Earth and in space, Nat. Catal. 2 (2019) 188–197, https://doi.org/10.1038/s41929-019-0244-4.
[52] P.A.U. Aldana, F. Ocampo, K. Kobl, B. Louis, F. Thibault-Starzyk, M. Daturi, P. Bazin, S. Thomas, A.C. Roger, Catalytic CO_2 volarization into CH_4 on Ni-based ceria-zirconia. Reaction mechanism by *operando* IR Spectroscopy, Catal. Today 215 (2013) 201–207, https://doi.org/10.1016/j.cattod.2013.02.019.
[53] Q. Pan, J. Peng, T. Sun, S. Wang, Insight into the reaction route of CO_2 methanation: promotion effect of medium basic sites, Catal. Commun. 45 (2014) 74–78, https://doi.org/10.1016/j.catcom.2013.10.034.
[54] C. Schild, A. Wokaun, A. Baiker, On the hydrogenation of CO and CO_2 over copper/zirconia and palladium/zirconia catalysts, Fresenius J. Anal. Chem. 341 (1991) 395–401, https://doi.org/10.1007/BF00321943.
[55] J. Ashok, M.L. Ang, S. Kawi, Enhanced activity of CO_2 methanation over Ni/CeO_2-ZrO_2catalysts: influence of preparation methods, Catal. Today 281 (2017) 304–311, https://doi.org/10.1016/j.cattod.2016.07.020.
[56] G.D. Weatherbee, C.H. Bartholomew, Hydrogenation of CO_2 on group VIII metals: VI. Specific activities and selectivities of silica-supported Co, Fe, and Ru, J. Catal. 87 (1984) 352–362, https://doi.org/10.1016/0021-9517(84)90196-9.
[57] F. Kovanda, T. Rojka, J. Dobešová, V. Machovič, P. Bezdička, L. Obalová, K. Jirátová, T. Grygar, Mixed oxides obtained from Co and Mn containing layered double hydroxides: preparation, characterization, and catalytic properties, J. Solid State Chem. 179 (2006) 812–823, https://doi.org/10.1016/j.jssc.2005.12.004.
[58] J. Jia, P. Zhang, L. Chen, The effect of morphology of α-MnO_2 on catalytic decomposition of gaseous ozone, Catal. Sci. Technol. 6 (2016) 5841–5847, https://doi.org/10.1039/c6cy00301j.
[59] P. Arnoldy, J. Moulijn, Temperature-programmed reduction of $CoOAl_2O_3$, J. Catal. 93 (1985) 38–54, https://doi.org/10.1016/0021-9517(85)90149-6.
[60] X. Niu, H. wie, K. Tang, W. Liu, G. Zhao, Y. Yang, Solvothermal synthesis of 1D nanostructured Mn_2O_3: effect of Ni^{2+} and Co^{2+} substitution on the catalytic activity of nanowires, RCS Adv. 5 (2015) 66271–66277, https://doi.org/10.1039/c5ra14618f.
[61] H. Kishimoto, K. Yamaji, M.E. Brito, T. Horita, H. Yokokawa, Gernalized Ellingham Diagramms for utilization in solid oxide fuel cells, J. Mining Metal. 44 (2008) 39–48, https://doi.org/10.2298/JMMB08081039K.
[62] J.I. Di Cosimo, V.K. Díez, M. Xu, E. Iglesia, C.R. Apesteguía, Structure and surface and catalytic properties of Mg-Al basic oxides, J. Catal. 178 (1998) 499–510, https://doi.org/10.1006/jcat.1998.2161.
[63] G. Busca, V. Lorenzelli, V. Sanchez Escribano, R. Guidetti, FT-IR study of the surface properties of the spinel $NiAl_2O_4$ and $CoAl_2O_4$ in relation to those of transitional aluminas, J. Catal. 131 (1991) 167–177, https://doi.org/10.1016/0021-9517(91)90333-Y.
[64] N. Kumar, K. Jothimurugesan, G.G. Stanley, V. Schwartz, J.J. Spivey, In situ FT-IR study on the effect of cobalt precursors on CO adsorption behavior, J. Phys. Chem. C 115 (2011) 990–998, https://doi.org/10.1021/jp104878e.
[65] T. Das, S. Sengupta, G. Deo, Effect of calcination temperature during the synthesis of Co/Al_2O_3 catalyst used fort he hydrogenation of CO_2, Reac. Kinet. Mech. Cat. 110 (2013) 147–162, https://doi.org/10.1007/s11144-013-0592-z.
[66] F.M.T. Mendes, C.A.C. Perez, F.B. Noronha, C.D.D. Souza, D.V. Cesar, H.J. Freund, M. Schmal, Fischer-Tropsch synthesis on anchored Co/Nb_2O_5/Al_2O_3 catalysts: the nature of the surface and the effect on chain growth, J. Phys. Chem. B 110 (2006) 9155–9163, https://doi.org/10.1021/jp060175g.
[67] J. Baltrusaitis, J.H. Jensen, V.H. Grassian, FTIR spectroscopy combined with isotope labeling and quantum chemical calculations to investigate adsorbed bicarbonate formation following reaction of carbon dioxide with surface hydroxyl groups on Fe_2O_3 and Al_2O_3, J. Phys. Chem. B 110 (2006) 12005–12016, https://doi.org/10.1021/jp057437j.